2005

Spectroscopy of KISS Emission-Line Galaxy Candidates. III. A Second Set of MDM Observations

Anna Jangren
Wesleyan University

Gary Wegner
Dartmouth College

John J. Salzer
Wesleyan University

Jessica K. Werk
Wesleyan University

Caryl Gronwall
Wesleyan University

The Astronomical Journal, 130:496–505, 2005 August

SPECTROSCOPY OF KISS EMISSION-LINE GALAXY CANDIDATES. III. A SECOND SET OF MDM OBSERVATIONS

Anna Jangren
Astronomy Department, Wesleyan University, Middletown, CT 06459; anna@astro.wesleyan.edu

Gary Wegner
Department of Physics and Astronomy, Dartmouth College, 6127 Wilder Laboratory, Hanover, NH 03755; gary.wegner@dartmouth.edu

and

John J. Salzer, Jessica K. Werk,[1] and Caryl Gronwall[2]
Astronomy Department, Wesleyan University, Middletown, CT 06459; slaz@astro.wesleyan.edu
Received 2005 February 24; accepted 2005 April 20

ABSTRACT

Spectroscopic observations for 315 emission-line galaxy (ELG) candidates from the KPNO International Spectroscopic Survey (KISS) have been obtained using the MDM Observatory 2.4 m telescope on Kitt Peak. KISS is a wide-field objective-prism survey for extragalactic emission-line objects that has cataloged over 2200 ELG candidates to date. Spectroscopic follow-up observations are being carried out to study the characteristics of the survey objects. The observational data presented here include redshifts, reddening estimates, line equivalent widths, Hα line fluxes, and emission-line ratios. The galaxies have been classified based on their emission-line characteristics. The procedure for selecting the ELG candidates in KISS is found to be very reliable: 93% of the candidates in this sample are verified to have emission lines. A comparison of objective-prism survey data—redshifts, Hα line fluxes, and equivalent widths—to the long-slit measurements shows good overall agreement.

Key words: galaxies: distances and redshifts — galaxies: Seyfert — galaxies: starburst — surveys

Online material: machine-readable tables

1. INTRODUCTION

The KPNO International Spectroscopic Survey (KISS) is an objective-prism survey designed to provide basic observational data for a large number of extragalactic emission-line sources. The survey has been carried out with the 0.61 m Burrell Schmidt telescope at Kitt Peak.[3] The use of a CCD detector distinguishes this survey from the classical photographic objective-prism surveys, allowing us to probe to much fainter flux levels. To date, KISS has identified 2271 emission-line objects. The specific details of the survey have been described in the first paper in this series (Salzer et al. 2000, hereafter Paper I). The first three survey lists are presented in Salzer et al. (2001, hereafter KR1; 2002, hereafter KB1) and in Gronwall et al. (2004b, hereafter KR2). Objects cataloged in KR1 and KR2 were selected by the presence of Hα in their objective-prism spectra, while the KB1 list surveyed the blue portion of the spectrum and detected objects via their [O III] λ5007 and/or Hβ lines. In a small fraction of the KISS emission-line galaxy (ELG) candidates ($\sim$2.5%), a shorter wavelength line is redshifted into the spectral bandpass of the objective-prism spectra.

Members of the KISS group have obtained long-slit spectra of KISS ELG candidates at several telescopes. To date we have obtained follow-up spectroscopy for 1625 of the ELG candidates, or over 70% of the survey sample. For the first two survey lists (KR1 and KB1) we have now obtained 100% complete follow-up. These observations allow for a more detailed spectroscopic analysis of the KISS emission-line objects. This paper is the third in a series that presents data from slit spectra for large numbers of KISS ELGs. It presents the data obtained for 315 objects over three seasons (2002–2004) at the MDM 2.4 m telescope. The results from earlier follow-up observations at MDM have been presented in Wegner et al. (2003). Spectroscopic observations carried out at other telescopes are presented in Gronwall et al. (2004a; Hobby-Eberly Telescope observations) and Salzer et al. (2005a; KPNO observations). The spectroscopic properties of the full samples of KISS ELGs will be presented in L. B. Chomiuk et al. (2005, in preparation) for KB1 and A. Jangren et al. (2005, in preparation) for KR1. As in Wegner et al. we present here a comparison of the MDM spectroscopic results with the properties derived from the objective-prism survey data listed in the KISS survey papers (KR1, KR2, and KB1). In § 2 we describe the selection of the sample, the observations, and the data reduction. The quantities measured in the long-slit spectra are presented in § 3, and in § 4 we compare these to the corresponding survey database properties. We summarize our conclusions in § 5.

2. OBSERVATIONS

We obtained spectra for 315 KISS objects at the MDM 2.4 m telescope over the course of three observing runs in 2002 April, 2003 April, and 2004 May. The observing run details are listed in Table 1. Column (1) lists the dates of the observations, and column (2) gives their run ID numbers, which are used for internal record keeping. The last digit indicates which night during a given observing run the observations were obtained, and the preceding digits denote the number of the observing run in our program of follow-up spectroscopic observations (e.g., run

[1] Current address: Department of Astronomy, University of Michigan, Ann Arbor, MI 48109; jwerk@umich.edu.
[2] Current address: Department of Astronomy and Astrophysics, Pennsylvania State University, University Park, PA 16802; caryl@astro.psu.edu.
[3] Survey carried out with the Burrell Schmidt telescope of the Warner and Swasey Observatory, Case Western Reserve University.

TABLE 1
MDM Spectroscopic Observing Runs

Date (1)	Run ID (2)	Conditions (3)	Number Observed (4)
2002 Apr 16.....	191	High humidity early	14
2002 Apr 17.....	192	Mostly clear	42
2002 Apr 18.....	193	Mostly clear	38
2003 Apr 8.....	291	Clear until end of night	37
2003 Apr 9.....	292	Clear, good spectrophotometry	38
2003 Apr 10.....	293	Clear until end of night	38
2004 May 21.....	341	Mostly clear, some haze	34
2004 May 22.....	342	Clear, good spectrophotometry	38
2004 May 23.....	343	Clear, good spectrophotometry	36
2004 May 24.....	344	Clouds; no data obtained	...

ID = 192 designates night 2 of KISS follow-up spectroscopy run 19). Column (3) indicates the sky conditions during the night, and column (4) lists the number of follow-up spectra that were obtained.

2.1. *Sample Selection*

As was the case with the samples of objects included in our previous spectroscopic follow-up papers (Wegner et al. 2003; Gronwall et al. 2004a), the objects selected for observation in the runs included in the current paper were not chosen at random from the objects in the KISS database. Rather, they were selected so as to provide follow-up spectra for a specific subsample of the KISS ELGs in order to allow us to carry out a specific project or type of analysis. Since the spectral characteristics of the overall data set presented here are defined by the makeup of the sample of galaxies observed, it is important to appreciate the sample definition. As we mention in §§ 3.2 and 4, the spectral properties of the current data set differ in modest ways from those of the Wegner et al. paper.

For the 2002 MDM run, our main focus was on obtaining spectra of ELGs from the KB1 survey list, since we were in the beginning stages of a project whose goal was to study the properties of the full [O III]-selected sample (L. B. Chomiuk et al. 2005, in preparation). In addition, we also used this run to complete our follow-up observations of radio-detected KISS ELGs from KR2 (see Van Duyne et al. 2004). During the 2003 MDM run, our primary focus was on observing all KR1 objects with *B* magnitudes brighter than 18.0 that had not yet been observed spectroscopically, while also obtaining spectra for candidate luminous compact blue galaxies for the project of Werk et al. (2004). In the most recent observing season, our goal was to complete the spectroscopic observations of all objects from the KR1 list, which we succeeded in doing. After the completion of the 2004 season, our group had obtained follow-up spectra for 100% of both the KR1 and KB1 lists. Complete details of the properties of the KISS ELGs from these two lists will be presented in a pair of forthcoming papers.

2.2. *Instrument Setup*

The instrumental setup and observing methods used were the same as for the previous MDM observations reported in Wegner et al. (2003). All observations were taken with the Mark III Spectrograph, using a slit width of 1.″68. The grating used had 300 grooves mm^{-1} and was blazed at 5400 Å, giving a reciprocal dispersion of 5.4 Å $pixel^{-1}$. The spectral range covered was 3900–8500 Å, although the spectrograph-CCD combination had very little sensitivity below ~4300 Å. The echelle CCD was used during all three runs, yielding a pixel scale along the slit of 0.″78 $pixel^{-1}$. All exposures were 10 minutes (600 s) long. Each night of observations included images of a HgNe lamp to set the wavelength scale, images in which the CCD was illuminated by a quartz flat-field lamp, and images of several spectrophotometric standard stars for flux calibration. The majority of our spectra were obtained under photometric conditions, although some objects were observed through thin clouds. Comparison of the observing run codes in the main data tables with the information given in Table 1 should allow the reader to ascertain the spectrophotometric integrity of any given object.

2.3. *Data Reduction*

The data reduction was carried out with the Image Reduction and Analysis Facility (IRAF).[4] Processing of the two-dimensional spectral images followed standard methods. The mean bias level was determined from the overscan region of each image and subtracted from the image. For each night, 10 zero-second exposures were average-combined to create a mean bias image, which was subtracted to correct the science images for any possible two-dimensional structure. To achieve flat-fielding we used a median-combined quartz lamp image that had been corrected for any wavelength-dependent response.

We extracted the one-dimensional spectra using the IRAF *noao.twodspec.apextract.apall* routine. The extraction width (i.e., distance along the slit) was selected independently for each source by running *apall* interactively. For most sources the emission region was unresolved spatially, so the extraction width was limited to ~5″–7″. This extraction region typically included >90% of the observed emission-line flux for each object. Sky subtraction was also performed at this stage, with the sky spectrum being measured in 25″–30″ wide regions on either side of the object.

The HgCdNe lamp spectra were used to assign a wavelength scale, and the spectra of the spectrophotometric standard stars were used to establish the flux scale. The standard star data were also used to correct the spectra of our target ELGs for telluric absorption. This is important for our ELGs, since for certain redshifts lines such as the [S II] doublet, [N II], or Hα could fall in the strong *B* band and lead to a severe underestimate of the true line flux. The emission-line fluxes and equivalent widths (EWs) were measured using the *noao.onedspec.splot* routine.

The resolution of the MDM spectra does not fully separate the Hα and [N II] λ6583 lines. We measured the total flux of the

[4] IRAF is distributed by the National Optical Astronomy Observatory, which is operated by the Association of Universities for Research in Astronomy (AURA), Inc., under cooperative agreement with the National Science Foundation.

TABLE 2
MDM Spectroscopic Data: 30° Red Survey

KISSR (1)	Field (2)	ID (3)	Run (4)	Q (5)	z (6)	$c_{H\beta}$ (7)	EW (Å) [O II] (8)	EW (Å) Hβ (9)	EW (Å) [O III] (10)	EW (Å) Hα (11)	Hα Flux[a] (12)	Flux Ratios[b] [O II]/Hβ (13)	Flux Ratios[b] [O III]/Hβ (14)	Flux Ratios[b] [N II]/Hα (15)	Flux Ratios[b] [S II]/Hα (16)	Type (17)
4.....	F1215	3026	342	3	0.06030	0.801	...	8.13	1.31	36.43	49.238	...	−0.7227	−0.3440	−0.5390	SBG
7.....	F1215	1851	341	3	0.08136	0.508	...	4.77	4.52	23.89	14.998	...	0.0042	−0.5856	−0.5747	SBG
21.....	F1215	430	343	2	0.06739	0.435	...	15.73	17.81	71.61	69.233	...	0.0642	−0.7737	−0.5998	SBG
36.....	F1220	2196	343	2	0.06410	0.611	...	8.17	17.87	33.79	27.191	...	0.3706	−0.7982	−0.5279	SBG
42.....	F1220	933	341	3	0.06136	0.632	...	7.92	19.40	43.43	16.630	...	0.4209	−1.2315	−0.5369	SBG
58.....	F1225	3658	291	3	0.05801	1.448	...	1.70	...	16.17	26.786	...	...	−0.3884	−0.6553	SBG
62.....	F1225	2947	342	2	0.06485	0.467	...	14.80	7.58	62.26	75.314	...	−0.2516	−0.4792	−0.5449	SBG
65.....	F1225	1570	292	3	0.05008	...	...	...	...	16.34	19.415	...	...	−0.3686	−0.4163	SBG
66.....	F1225	1544	341	2	0.08483	1.178	...	4.79	6.84	38.81	49.802	...	0.1366	−0.2911	−0.5470	SBG
79.....	F1230	257	293	3	0.06380	...	...	...	...	13.39	15.076	...	...	−0.3257	−0.4446	SBG

Note.—Table 2 is published in its entirety in the electronic edition of the *Astronomical Journal*. A portion is shown here for guidance regarding its form and content.
[a] In units of 10^{-16} ergs s^{-1} cm^{-2}.
[b] In logarithmic units.
[c] Observation made under nonphotometric conditions.

blended line complex, the peak flux ratio of the Hα and [N II] lines, and the line positions. On the basis of these data we then separated the lines with a deblending routine to determine the Hα flux and the [N II]/Hα ratio. In a few cases the [N II] line was too weak to be visible, except as a broadened "wing" on the red side of Hα; we did not attempt to deblend the lines in such objects.

The decimal reddening coefficient $c_{H\beta}$ (defined in eq. [1]) was calculated based on the measured ratio of Hα to Hβ flux, assuming an intrinsic ratio of 2.86 and an electron temperature of $T_e = 10,000$ K. If the [O III] λ4363 line flux was measured, our analysis program used this to iterate a new value for both T_e and the intrinsic Hα/Hβ ratio. The measured line ratios were then corrected for reddening using $c_{H\beta}$, following the standard prescription (e.g., Osterbrock 1989)

$$\frac{I(\lambda)}{I(\mathrm{H}\beta)} = \frac{F(\lambda)}{F(\mathrm{H}\beta)} \exp\left[c_{\mathrm{H}\beta} f(\lambda)\right], \quad (1)$$

where f has been measured from studies of absorption in the Milky Way. For seven objects the measured Hα/Hβ ratio yields a negative value for $c_{H\beta}$. In the majority of these cases the formal error in $c_{H\beta}$ is such that the measured value is consistent with $c_{H\beta} = 0.00$. Whenever a negative $c_{H\beta}$ was measured, $c_{H\beta} = 0.00$ was used for the computation of reddening-corrected line ratios. The measured (negative) $c_{H\beta}$ values are listed in the tables.

3. KPNO INTERNATIONAL SPECTROSCOPIC SURVEY: LIST OF MDM FOLLOW-UP SPECTROSCOPY

3.1. *The Spectroscopic Data*

In Tables 2–4 we present the results of our spectroscopic observations of the 2002–2004 MDM sample. The tables are organized by the KISS source catalogs in which the targets are located. Table 2 lists the spectral data for KISS ELGs from the first red survey list (30° Red Survey; KR1), Table 3 presents the results for objects from the second red survey list (43° Red

TABLE 3
MDM Spectroscopic Data: 43° Red Survey

KISSR (1)	Field (2)	ID (3)	Run (4)	Q (5)	z (6)	$c_{H\beta}$ (7)	EW (Å) [O II] (8)	EW (Å) Hβ (9)	EW (Å) [O III] (10)	EW (Å) Hα (11)	Hα Flux[a] (12)	Flux Ratios[b] [O II]/Hβ (13)	Flux Ratios[b] [O III]/Hβ (14)	Flux Ratios[b] [N II]/Hα (15)	Flux Ratios[b] [S II]/Hα (16)	Type (17)
1154.....	F1155	1892	192	2	0.07195	...	...	...	10.97	9.60	23.810	...	...	0.0193	−0.3872	Sy2
1210.....	F1204	1728	343	3	0.04838	1.209	...	2.93	...	22.40	46.906	...	...	−0.6219	−0.6870	SBG
1220.....	F1208	1912	192	3	0.03685	0.960	...	2.78	4.56	19.25	19.828	...	0.1861	−0.4437	−0.3438	SBG
1221.....	F1208	1840	192	3	0.03721	1.444	...	1.45	3.96	13.32	26.715	...	0.3927	−0.2711	−0.4557	LIN
1234.....	F1212	4933	293	3	0.02375	...	...	...	...	...	...	...	...	...	...	Gal
1239.....	F1212	2759	293	3	0.03975	2.603	...	0.69	0.69	15.68	49.652	...	−0.0652	−0.4190	−0.7692	SBG
1248.....	F1212	1077	293	1	0.02422	0.560	...	14.31	15.97	86.84	216.230	...	0.0148	−0.5982	−0.5933	SBG
1251.....	F1212	557	293	2	0.02421	1.727	...	1.13	3.01	13.15	131.173	...	0.3976	−0.4180	−0.3590	SBG
1284.....	F1221	6380	342	3	0.06741	...	...	...	...	2.92	18.387	...	...	0.1442	...	LIN
1307.....	F1229	6309	193	1	0.00063	0.518	...	8.00	27.33	52.52	1560.488	...	0.5238	−0.9542	−0.7312	SBG

Note.—Table 3 is published in its entirety in the electronic edition of the *Astronomical Journal*. A portion is shown here for guidance regarding its form and content.
[a] In units of 10^{-16} ergs s^{-1} cm^{-2}.
[b] In logarithmic units.

TABLE 4
MDM Spectroscopic Data: 30° Blue Survey

KISSB (1)	Field (2)	ID (3)	Run (4)	Q (5)	z (6)	$c_{H\beta}$ (7)	EW (Å) [O II] (8)	EW (Å) Hβ (9)	EW (Å) [O III] (10)	EW (Å) Hα (11)	Hα Flux[a] (12)	Flux Ratios[b] [O II]/Hβ (13)	Flux Ratios[b] [O III]/Hβ (14)	Flux Ratios[b] [N II]/Hα (15)	Flux Ratios[b] [S II]/Hα (16)	Type (17)
2.....	F0830	1711	193	2	0.04511	0.059	...	16.72	54.33	91.12	22.291	...	0.5062	−1.3093	−0.6103	SBG
3.....	F0835	905	193	1	0.07876	0.773	...	8.40	28.64	57.63	66.051	...	0.5095	−0.8906	−0.5301	SBG
6.....	F0840	1805	192	1	0.01805	0.514	...	10.51	32.79	65.43	40.095	...	0.4763	−0.9308	−0.4979	SBG
8.....	F0845	1172	192	1	0.02719	0.171	...	33.82	129.30	175.30	118.157	...	0.5746	−1.2371	−0.6580	SBG
13.....	F0900	1510	192	1	0.02278	0.970	...	4.29	8.95	31.51	104.408	...	0.2921	−0.6434	−0.4884	SBG
21.....	F0930	1460	192	1	3.42140	...	...	...	...	...	...	...	...	...	...	QSO
26.....	F0940	776	193	2	...	...	...	...	...	...	...	...	...	...	...	Star
33.....	F1010	4233	192	1	0.03432	0.425	...	16.64	53.28	93.47	177.576	...	0.4926	−0.8931	−0.6589	SBG
34.....	F1015	2032	192	2	0.01428	0.732	...	4.64	23.74	36.83	14.506	...	0.6732	−1.1780	−0.8446	SBG
37.....	F1030	1463	192	1	0.07902	−0.029	62.84	42.10	177.10	166.73	69.796	0.3167	0.6202	−1.1542	−0.6649	SBG

Note.—Table 4 is published in its entirety in the electronic edition of the *Astronomical Journal*. A portion is shown here for guidance regarding its form and content.
[a] In units of 10^{-16} ergs s^{-1} cm^{-2}.
[b] In logarithmic units.

Survey; KR2), and Table 4 lists the data for the blue survey list (30° Blue Survey; KB1). All three tables have precisely the same format; the contents are as follows: Column (1) gives the survey ID number (KISSR for the red surveys, KISSB for the blue survey). Table 5 correlates the KISSR and KISSB ID numbers for those objects included in both survey lists (see below). Column (2) lists the survey field designation and column (3) the field ID number. These two quantities give alternate identifications for the KISS ELGs that are used internally with the KISS database. Column (4) identifies the observing run during which the spectrum was obtained (see Table 1). Column (5) gives a coarse spectral quality code: $Q = 1$ refers to high-quality spectra with high signal-to-noise ratio (S/N) emission lines and reliable emission-line ratios, $Q = 2$ is assigned to spectra of lesser quality that still have reliable line ratios, and $Q = 3$ refers to spectra in which the data are of low quality, usually because of the faintness of the object and/or the weakness of the emission lines (see Fig. 1 for examples). Column (6) gives the redshift of each object determined from the average of the redshifts derived from all strong emission lines. Typical formal uncertainties for z are 0.00010–0.00025 (30–75 km s^{-1}). Column (7) lists the decimal reddening coefficient $c_{H\beta}$. Columns (8)–(11) present the observed EWs of [O II] $\lambda\lambda$3726, 3729, Hβ, [O III] λ5007, and Hα. The Hα flux, in units of 10^{-16} ergs s^{-1} cm^{-2}, is listed in column (12). These values should be treated with caution, since the observing conditions at MDM were not always photometric; see Table 1 for

TABLE 5
KISSB-KISSR Correlation

KISSB (1)	KISSR (2)	Field (3)	ID (4)
101.....	86	F1235	1358
110.....	149	F1255	3653
111.....	151	F1255	3490
130.....	268	F1320	4207
134.....	289	F1325	2252
140.....	343	F1340	1892
148.....	413	F1355	637
153.....	456	F1405	2697
163.....	525	F1420	4537
165.....	538	F1420	2034
178.....	614	F1500	4973
181.....	626	F1505	5024
184.....	654	F1510	3951
190.....	715	F1520	1641
206.....	966	F1605	6609
208.....	978	F1605	2241
213.....	1036	F1625	2584

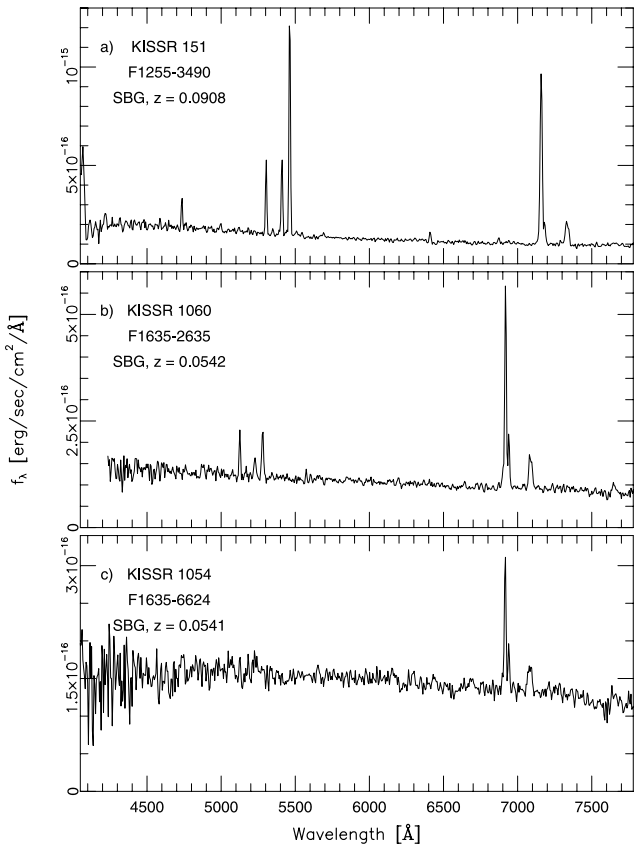

Fig. 1.—Sample MDM spectra of different spectral quality Q. (*a*) $Q = 1$. The line ratios [O III]/Hβ, [N II]/Hα, and [S II]/Hα can all be accurately determined. [He I] λ5876 and [O I] λ6300 can be identified. (*b*) $Q = 2$. The S/N is lower, but the main line ratios are still reliable. (*c*) $Q = 3$. The line ratios that are measured have a lower degree of accuracy.

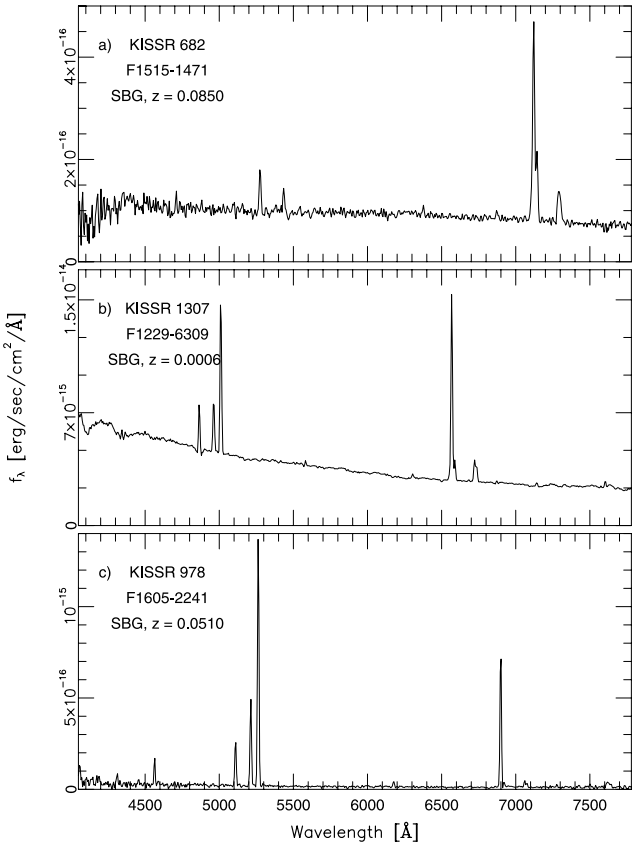

FIG. 2.—Sample MDM spectra of star-forming galaxies. All have spectral quality $Q = 1$. The spectra are ordered by increasing degree of excitation, as shown by their [O III] λ5007/Hβ ratios. As [O III]/Hβ increases, [N II]/Hα and [S II]/Hα decrease. (*a*) Low-excitation starburst; [O III]/H$\beta \sim 0.5$, and [N II]/H$\alpha \sim 0.3$. (*b*) Medium-excitation starburst; [O III]/H$\beta \sim 3$, and [N II]/H$\alpha \sim$ 0.1. This nearby object is the well-known starburst galaxy NGC 4449. (*c*) High-excitation starburst spectrum with [O III]/H$\beta \sim 5$, similar to what is seen for many Seyfert 2 galaxies. However, its [N II]/Hα ratio is only $\sim$0.03.

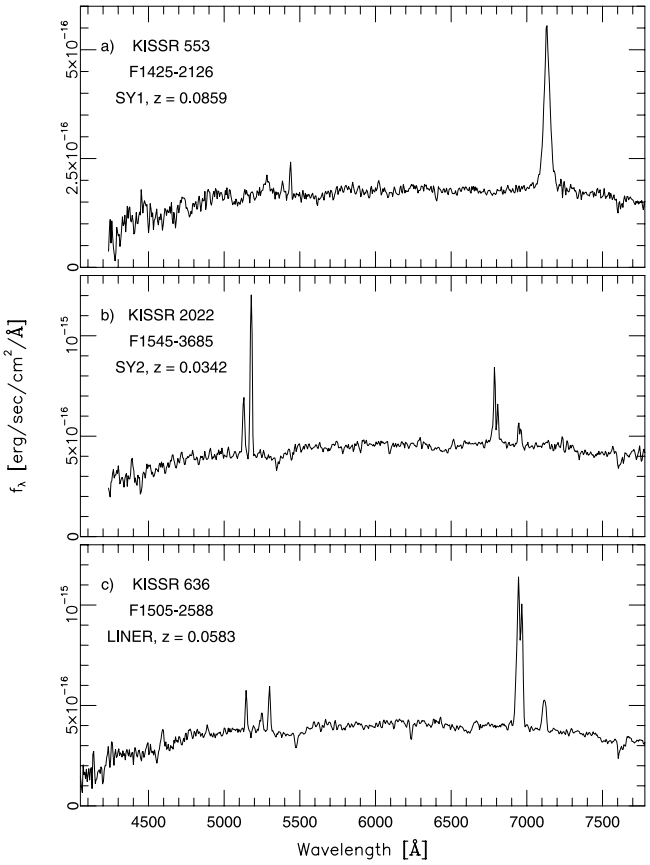

FIG. 3.—Sample MDM spectra of active galaxies. All have spectral quality $Q = 2$. (*a*) The broadened Hα line is the strongest line in this Seyfert 1 spectrum. The narrow lines of the [O III] doublet are also visible. (*b*) In this Seyfert 2 spectrum the strongest lines belong to the [O III] doublet, while Hβ is so weak that it is difficult to measure. The [N II] λ6583 line is nearly as strong as Hα. Several absorption features are clearly visible. (*c*) In this LINER spectrum, Hβ and the [O III] λ5007 line are of comparable strength. The [N II] λ6583 line is nearly as strong as Hα. Strong magnesium and sodium absorption features can also be seen.

details. Columns (13)–(16) give the logarithms of the reddening-corrected line ratios [O II] $\lambda\lambda$3726, 3729/Hβ, [O III] λ5007/Hβ, [N II] λ6583/Hα, and [S II] $\lambda\lambda$6717, 6731/Hα. If an EW or line ratio measurement is not listed, either the relevant line was not present in the spectrum (often because of low S/N) or the line is redshifted out of the region covered by our spectra. For most of the objects observed at MDM, the [O II] doublet was not present in our observed spectral range. This is due to the lack of throughput of the spectrograph optics at wavelengths below 4000 Å.

Finally, column (17) indicates the activity type for each object. We identify eight classes: SBG = starburst galaxy, SY1 = Seyfert 1, SY2 = Seyfert 2, LIN = low-ionization nuclear emission region (LINER), QSO = quasi-stellar object, H II = H II region within a galaxy, Gal = non-ELG, and Star = Galactic star. The latter two categories represent objects that were mistakenly identified by the survey as ELGs; they are not actual extragalactic emission-line sources. The H II category represents a small number of KISS objects that were originally believed to be unique emission-line systems, based on the survey data. Subsequent observations revealed them to be normal (albeit quite bright) H II regions within the disks of spiral galaxies. They are usually located on the outskirts of the spiral disk, and hence it was unclear from the survey data whether they were separate dwarf companions to the larger spiral, background objects, or part of the disk. Since the survey has purposely tried to avoid cataloging normal H II regions located within spiral disks, they only appear when their status is ambiguous in the survey data. Finally, note that all objects whose spectra indicate photoionization by hot stars are cataloged as SBGs, regardless of their nature. We do not attempt to subclassify SBGs into other categories of star-forming galaxies (e.g., blue compact dwarfs or H II galaxies), since such classifications are both highly subjective and dependent on the type of data used.

In the sample of 315 objects observed with the MDM presented in this paper, there are 227 objects from the first red survey list (KR1), 30 objects from the second red survey list (KR2), and 75 objects from the blue survey list (KB1). Note that Tables 2 and 4 contain data for 17 objects in common (see Table 5). Since KR1 and KB1 overlap in terms of sky coverage, many ELG candidates are detected in both surveys (which use independent spectral data). It was decided to include the spectral data for the objects that are duplicated in the two survey lists in both data tables. This way, a reader attempting to locate information about a specific KISSB object will not be forced to cross-check the KB1 catalog with KR1.

In Figures 1–5 we present some characteristic spectra of objects observed with the MDM 2.4 m telescope to illustrate the range of objects identified by KISS. Three starburst galaxy spectra of different Q-values show the range of spectral quality in the sample (Fig. 1). Figure 2 shows three star-forming galaxies with varying degrees of ionization, as indicated by the [O III] λ5007/Hβ

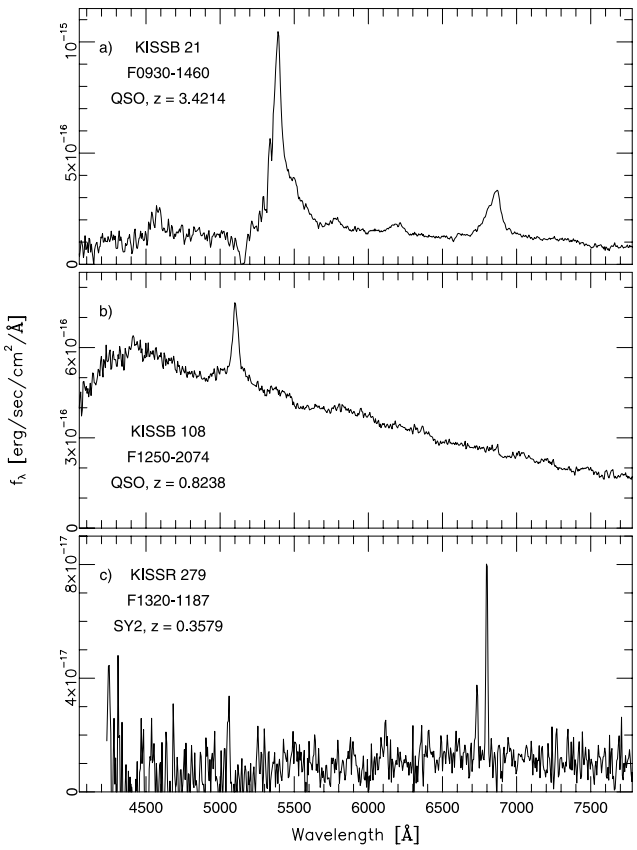

FIG. 4.—MDM spectra of moderate- and high-redshift sources. (*a*) The two strongest features seen in this QSO spectrum are Lyα and C IV. (*b*) The strong line in this QSO spectrum is identified as Mg II. (*c*) The [O III] doublet is clearly visible in the spectrum of this moderate-*z* Seyfert 2 galaxy.

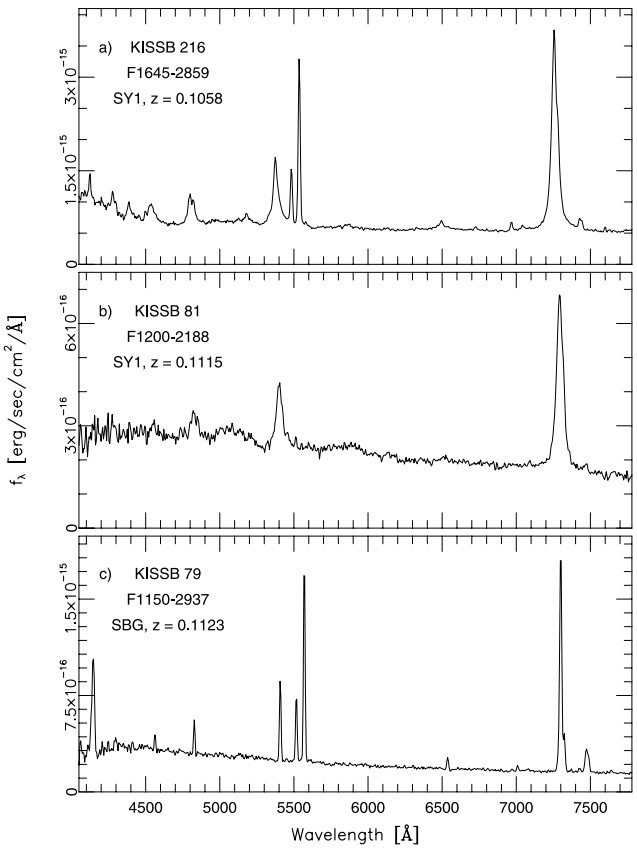

FIG. 5.—MDM spectra of three blue survey objects in which Hβ, rather than the [O III] λ5007 line, was detected in the objective-prism spectra. (*a*) In this Seyfert 1 spectrum both the narrow lines of the [O III] doublet and the broadened Hβ line can be seen. The blue survey filter throughput drops rapidly beyond $\lambda \sim 5500$ Å, and only the Hβ line can thus be detected in the objective-prism spectrum. (*b*) This Seyfert 1 galaxy has strong hydrogen lines, while the narrower forbidden lines are barely visible. (*c*) This starburst galaxy has strong [O III] lines; however, they fall beyond the survey filter cutoff. The Hβ line is located just blueward of the cutoff.

ratio. Figure 3 shows example spectra of Seyfert 1 and Seyfert 2 galaxies and a typical LINER source. Two QSOs at high redshift are shown in Figure 4, along with one Seyfert 2 galaxy at moderate redshift ($z \sim 0.36$). These are all examples of objects identified by KISS in which an emission line other than the targeted one has redshifted into the survey spectral region. In the case of the two QSOs, the Lyα and Mg II lines are seen in the blue objective-prism spectra of KB1, while for the Seyfert 2, [O III] λ5007 appears in the red spectral region of KR1, mimicking an Hα-selected ELG. About 2.5% of the KISS galaxies with follow-up spectra fall into this category, most of them active galactic nuclei (AGNs). A more complete discussion of the AGN population found in the KISS catalogs is given in Gronwall et al. (2002) and Stevenson et al. (2002). Finally, Figure 5 shows the spectra of the three objects from the blue survey list in which the detected emission line turned out to be Hβ rather than [O III] λ5007. Two of these are Seyfert 1 galaxies, and one is a starburst galaxy.

3.2. *Classification*

Emission-line objects detected by KISS span a wide range of object types, from star-forming dwarf galaxies to AGNs. The survey objective-prism spectra cannot be used to classify the objects according to the nature of the source of the ionizing radiation; their resolution is too low, and they cover only the spectral range 6400–7200 Å for KR1 and KR2 (see Fig. 2 of KR1 for some examples of objective-prism spectra) and 4800–5500 Å for KB1. It is, however, often possible to make a tentative classification of an ELG simply by looking at its long-slit spectrum. Seyfert 1 galaxies, for instance, are easily recognized from the broadening of their permitted lines. The MDM spectra have the lowest dispersion of all the spectroscopic follow-up observations, causing the [N II] λ6583 line to blend with Hα and the [S II] $\lambda\lambda$6717, 6731 doublet to be blended as well. Still, the dispersion is high enough for ELG classification (see Figs. 2 and 3) and for the measurement of crucial emission-line ratios.

The line ratios allow us to plot diagnostic diagrams that give a clear separation of different types of ELGs (see, e.g., Baldwin et al. 1981; Veilleux & Osterbrock 1987), which we use to verify our object classifications. In Figure 6 we plot log ([O III] λ5007/Hβ) against log ([N II] λ6583/Hα) for all MDM sample objects classified as starburst galaxies or AGNs with follow-up spectra of quality code $Q = 1$ or 2. As expected from models for starburst-powered ELGs of various metallicities, most objects fall along a sequence that arcs across the diagram. The solid line indicates the positions of H II region models of different metallicities (Dopita & Evans 1986). Low-metallicity starbursts are found in the upper left portion of the diagram and high-metallicity starbursts in the lower right. Objects powered by an AGN—Seyfert 2 galaxies and (presumably) LINERs—have higher values of [N II] λ6583/Hα and are located in the upper right portion of the diagram. Not included in the diagram are the moderate-redshift AGNs, since their observed spectra lack the [N II] λ6583/Hα ratio (their Hα and [N II] lines were redshifted out of our spectral range).

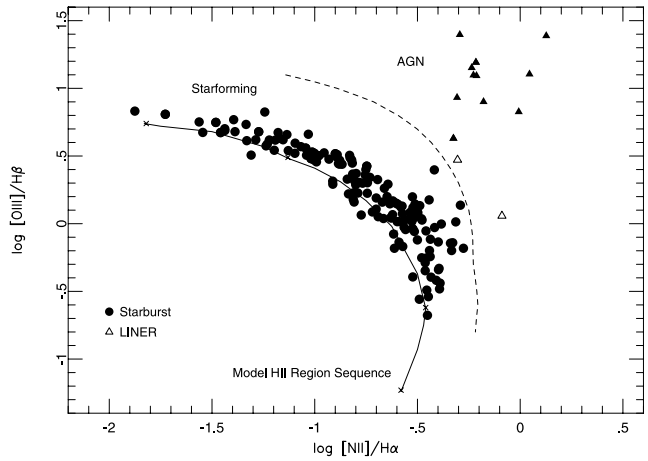

FIG. 6.—Line diagnostic diagram showing the relationship between the [N II] λ6583/Hα line ratio and the [O III] λ5007/Hβ line ratio. Only objects with spectral quality of $Q = 1$ or 2 were included in the diagram. Objects classified as starburst galaxies (SBGs) are shown as circles, LINERs as open triangles, and Seyfert 2 galaxies as filled triangles. Nearly all LINERs have spectral quality of $Q = 3$ and are not shown here. The dashed line roughly separates the star-forming galaxies from the active galaxies. The solid line represents an H II model sequence at various metallicities, from 0.1 $Z_\odot$ at the upper left to 2 $Z_\odot$ at the lower right (Dopita & Evans 1986).

Of the 315 objects with follow-up spectra obtained at MDM, the majority, 250 objects (79%), are classified as starburst galaxies (SBGs) of some type. This category includes a diverse range of star-forming galaxies, such as starburst nuclei galaxies, H II galaxies, irregular galaxies with significant star formation, and blue compact dwarfs. Since KISS detects a significant number of objects with Hα + [N II] emission-line EWs smaller than 30 Å, the SBG class also includes some intermediate- to late-type spiral galaxies (Kennicutt & Kent 1983; Kennicutt 1992). Active galaxies make up 13% of the sample: four objects are Seyfert 1 galaxies, 15 are Seyfert 2 galaxies, 21 are LINERs, and two are QSOs at redshifts of 0.82 and 3.42. This fraction of active galaxies is smaller than what was found for the set of objects observed with MDM during the first four seasons (Wegner et al. 2003). The difference is due to the specifics of the sample selection for the MDM observations during the early seasons, when we focused on KISS galaxies that were present in X-ray, far-infrared, or radio surveys and on objects that had the highest Hα luminosities. This selection effect is also noticeable when we compare Figure 6 to the corresponding figure in Wegner et al. In the present sample there is a paucity of high-metallicity star-forming galaxies, which are found at the lowest values of the [O III] λ5007/Hβ ratio. The sample presented here has a median survey line flux that is nearly 50% lower than that of the MDM sample from the earlier seasons; on average, higher flux objects tend to be more luminous and have higher metallicity.

Of the remaining 23 objects, all but one are non-ELGs: 15 are Galactic stars, and seven are galaxies with no emission lines in the wavelength region included in the objective-prism spectra. One object is an H II region in a nearby galaxy. To date, our follow-up spectroscopy has shown that $\sim$9% of the objects cataloged in KISS are actually non-ELGs. The non-ELGs cannot be distinguished from the bona fide ELGs based on survey data alone; however, their overall survey properties differ in some respects from those of the bulk of the ELGs. The objective-prism fluxes of non-ELGs are lower than for the confirmed ELGs, and their $B - V$ colors tend to be redder; roughly 60% of the sources with $B - V > 1.1$ are non-ELGs. The reddest confirmed ELGs are dominated by various types of AGNs, which make up nearly two-thirds of the bona fide ELGs with $B - V > 1.1$. Confirmed ELGs also tend to have brighter magnitudes than the non-ELG sources; for confirmed ELGs the median magnitude is $B \sim 17.8$, while for non-ELGs it is only $B \sim 19.4$. The ELGs and non-ELGs have similar distributions of objective-prism EWs and redshifts. A more complete discussion of the properties of the false detections is given in A. Jangren et al. (2005, in preparation).

The survey properties of the objects observed at MDM during the past three seasons (the second MDM sample) differ only marginally from the properties of the entire KISS catalog. The first and second Hα-detected survey lists have median apparent magnitudes of $B = 18.13$ and 18.08 mag, respectively, and the [O III]-selected survey list has a median magnitude of $B = 18.17$. The second MDM sample has a median apparent magnitude of $B = 17.95$ mag and is thus somewhat brighter. This is to be expected, since the faintest objects were preferentially observed with the Hobby-Eberly Telescope (Gronwall et al. 2004a). The KR1 and KR2 survey objects in the second MDM sample have a median color of $B - V = 0.66$. This value is very close to those of the overall Hα-detected survey lists, which have median colors of $B - V = 0.67$ and 0.69, respectively. The [O III]-selected survey list has a median color of $B - V = 0.50$. The median Hα + [N II] line flux of the second MDM sample agrees well with that of the full KISS catalog, while the median EW is $\sim$10% lower. This difference is also expected, since the objects with the largest EWs tend to be fainter and thus are not included in the samples observed at MDM. No significant difference is seen in the redshift distribution of the second MDM sample compared to the redshift distribution of the entire survey; both have a median redshift of $z \sim 0.06$.

4. COMPARISON OF SURVEY AND FOLLOW-UP SPECTROSCOPIC PROPERTIES

The KISS database contains a wealth of information for a large sample of ELG candidates and can potentially be used for a wide range of galaxy studies. The objective-prism spectral data, however, are inherently uncertain; their resolution is low, and they cover only a limited spectral range. Follow-up spectroscopy allows us to explore the reliability of survey measurements. As in Wegner et al. (2003) we compare three characteristics derived from the objective-prism survey spectra to their long-slit counterparts: redshifts, Hα EWs, and Hα line fluxes.

All objects detected by KISS have been assigned an estimated redshift based on the survey objective-prism data. The follow-up spectroscopy made it possible to check how well the prism redshifts correspond to redshifts obtained from higher resolution slit spectra. Figure 7 shows a comparison of the two types of redshifts. The overall agreement is good; out of the 315 objects observed, only 27 were found to have redshifts substantially different from the prism estimates ($\Delta v > \pm 4000$ km s^{-1}). Three of these were blue survey objects in which the Hβ line was interpreted as the [O III] λ5007 line (see Fig. 5), and one was a moderate-redshift red survey AGN in which the [O III] λ5007 line was redshifted to the bandpass covered by the red KISS objective-prism data and misidentified as Hα emission from a nearby dwarf galaxy (see Figs. 7*b* and 4*c*). A further two red survey objects were found to be high-redshift QSOs with strong lines in the wavelength region covered by the survey filter (see Figs. 4*a* and 4*b*). The resolution of the objective-prism spectra was too low to allow us to distinguish these cases from the survey data alone; the only way to identify them was through follow-up spectroscopy. Among the objects with discrepant survey redshifts were 14 Galactic stars that were initially identified as extragalactic objects and generally had survey redshifts in the range

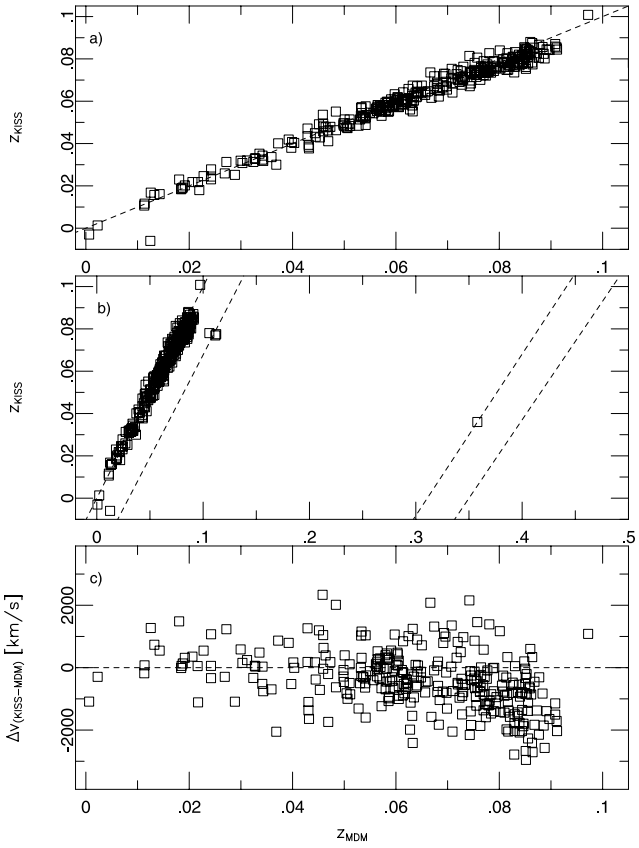

FIG. 7.—Comparison of objective-prism redshifts to long-slit redshifts. Objects determined to be Galactic stars or non-ELGs have been excluded from the plots. (*a*) Overall, there is good agreement between objective-prism redshifts (z_{KISS}) and the redshifts determined from the follow-up long-slit spectroscopy (z_{MDM}). (*b*) The dashed line in the left portion of the diagram shows the expected position of blue survey objects for which the Hβ line was misidentified as [O III] λ5007 emission in the objective-prism spectra. The three objects shown in Fig. 5 fall on or near this line. The dashed lines in the right portion of the diagram show the expected positions of red survey objects for which either [O III] λ5007 (*left line*) or Hβ (*right line*) of a moderate-redshift source was misidentified as Hα emission. Only one object, shown in Fig. 4, was detected by the red survey because of its strong [O III] λ5007 line. (*c*) The velocity difference Δv shows a relatively large scatter. The small offset toward negative values indicates that the survey redshifts tend to be somewhat lower than their long-slit counterparts. Above $z_{MDM} = 0.07$, the effect of the survey filter cutoff becomes apparent: the objective-prism redshifts are systematically lower than the long-slit redshifts, and this difference increases with redshift.

$z = 0.07$–0.08. Six objects were galaxies without emission lines, which were included as ELG candidates as a result of spurious features or noise. Finally, the star-forming galaxy KISSB 172 was assigned a slightly negative survey redshift but had a follow-up redshift of $z = 0.012$. The follow-up spectrum showed only weak blue lines, but the objective-prism spectrum showed a strong line blueward of the expected rest-frame position of Hα. This is a nearby, extended galaxy with a strong emission region that is offset from the center in the north-south direction. As described in KR2, a spatial offset in the north-south direction can lead to an unreliable objective-prism redshift estimate. For all other objects, in which the objective-prism redshift is actually based on a detection of the Hα line (for the red survey objects) or the [O III] λ5007 line (for the blue survey objects), the prism redshifts are comparable to those determined from the follow-up spectra.

Objects with redshifts $z > 0.07$, close to the filter-imposed redshift limit, tend to have objective-prism redshifts that are systematically lower than the redshifts determined from their long-slit spectra. As can be seen in Figure 7*c*, the difference increases with redshift. This effect arises when the broad line in the objective-prism spectrum falls near the wavelength cutoff of the survey filter; only the shorter wavelength part of the line is then detected, giving the impression of a weaker line at lower redshift. As described in Paper I, a correction for this effect was applied to the high-redshift portion of the first red survey list (KR1).

Using the corrected objective-prism redshifts, and including only those objects whose KISS redshifts were based on detection of the Hα line, we find that the velocity difference Δv has a scatter of $\sigma = \pm 870$ km s^{-1}. This number is consistent with expectations based on the accuracy of the objective-prism redshifts, which have reciprocal dispersions of 24 Å pixel^{-1} (KR1) and 17 Å pixel^{-1} (KR2) at Hα. The survey redshifts tend to be slightly lower than their counterparts measured with a slit. The offset corresponds to a mean velocity difference of $\sim$245 km s^{-1}, which is of the same order of magnitude as the scatter (0.28 σ). We get very similar results when we exclude the objects whose objective-prism redshifts were corrected (KR1 objects with $z > 0.07$); the mean velocity difference Δv is then somewhat greater, $\sim$278 km s^{-1}, and the scatter drops to $\sigma = \pm 838$ km s^{-1}.

We compared the redshifts of 32 objects that have data from both MDM long-slit spectroscopy and Century Redshift Survey (CRS) observations (Wegner et al. 2001). The two data sets show good agreement, with no apparent systematics. The MDM redshifts are slightly lower than the CRS redshifts, corresponding to a median offset of 26 km s^{-1}. The standard deviation is 67 km s^{-1}. It should be noted that the CRS redshifts were not determined from the emission lines alone; the software used to extract the redshifts also employed a cross-correlation algorithm for the absorption-line features (Thorstensen et al. 1989). The CRS redshifts can thus in some cases be independent of the emission-line features.

We also wished to see how well the Hα EWs and line fluxes derived from the red survey objective-prism spectra agree with those we measured in the follow-up spectra. For the flux comparison we only included the line fluxes of objects for which the follow-up observations were carried out under spectrophotometric conditions. All objects were included for the EW comparison. In the low-resolution prism spectra the [N II] lines were completely blended with the Hα line, but in the MDM spectra these lines were partly resolved. As described in § 2.3, measurements of the individual line fluxes are possible using a deblending routine. For the purpose of this comparison, we used the [N II] λ6583/Hα flux ratio determined from the MDM spectra to correct the prism spectra EWs and fluxes, effectively subtracting the [N II] contribution.

Plotting the [N II]-corrected objective-prism fluxes versus their long-slit counterparts shows them to be in overall agreement (see Fig. 8*a*). However, the line fluxes that we estimated from objective-prism spectra were generally $\sim$50% higher than those we measured in the MDM long-slit spectra. Since the objective-prism spectra sample a larger spatial region than the long-slit spectra, it is natural that they include a greater amount of flux for all extended sources. In Wegner et al. (2003) we showed that for the objects observed at MDM during the first four seasons there is a tendency for the objects with the highest objective-prism fluxes to have less of an offset from the long-slit fluxes than the bulk of the sample. Although the sample presented here does not contain as many high-flux objects as that in Wegner et al., we can see a hint of the same trend. This could indicate that the objects with higher objective-prism fluxes correspond to sources with smaller apparent sizes (i.e., powerful point sources as opposed to extended emission regions). Plotting

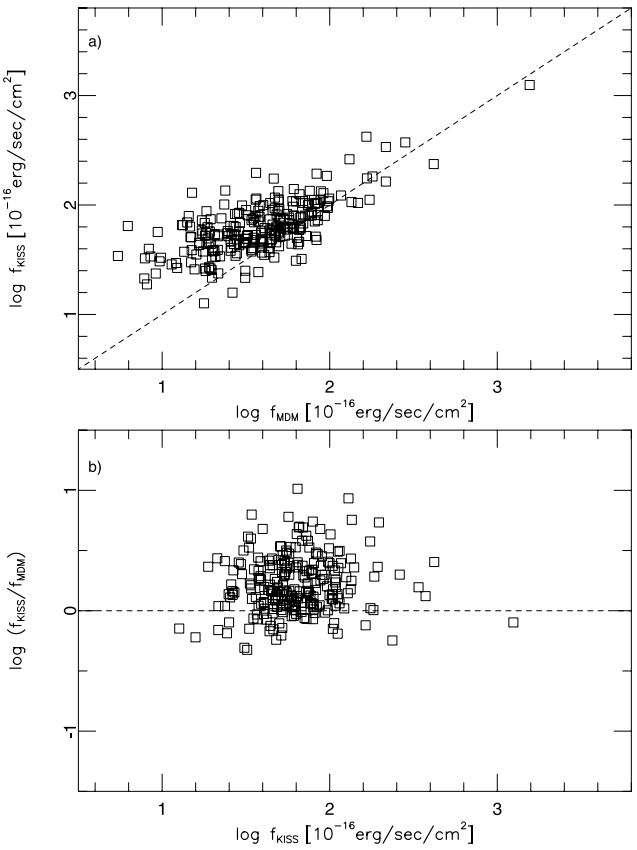

FIG. 8.—Comparison of corrected objective-prism Hα line fluxes f_{KISS} to long-slit fluxes f_{MDM}. (*a*) Relation $f_{KISS} = f_{MDM}$ (*dashed line*). Overall, there is a clear correlation between the two, but the objective-prism fluxes tend to be higher than the long-slit fluxes. This is expected, since the objective-prism spectra include flux from a larger spatial region than the long-slit spectra. (*b*) Line-flux ratio f_{KISS}/f_{MDM} vs. f_{KISS}. The dashed line indicates $f_{KISS}/f_{MDM} = 1$. In spite of a large scatter, 65% of the sample falls within $0.50 < f_{KISS}/f_{MDM} < 2$.

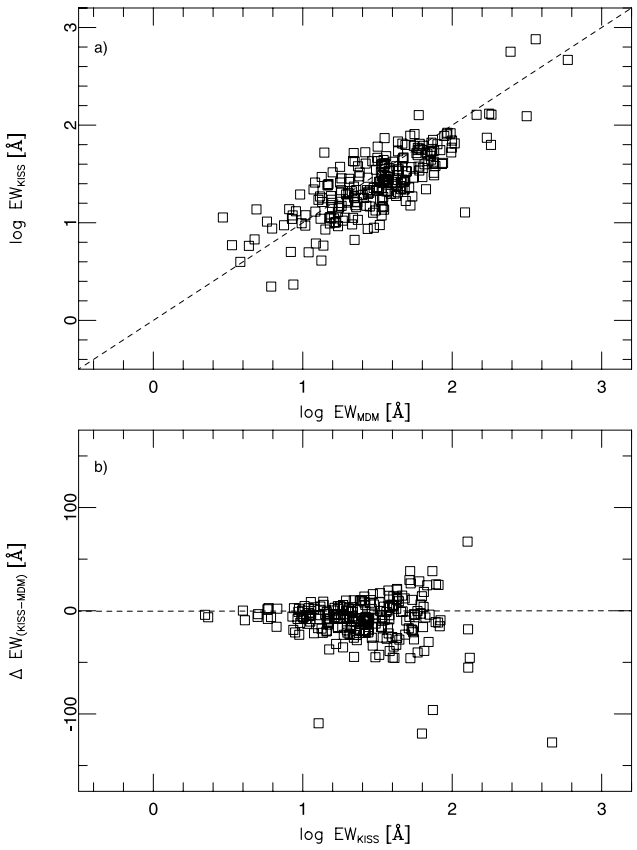

FIG. 9.—Comparison of corrected objective-prism Hα EWs (EW_{KISS}) to long-slit EWs (EW_{MDM}). (*a*) An overall correlation is seen between the two EWs, with no offset toward higher or lower values for either. The dashed line indicates $EW_{KISS} = EW_{MDM}$. Again, since the objective prism spectra sample a larger spatial region than the long-slit spectra, we do not expect an exact correspondence between EWs measured in each spectra. The difference in distribution of continuum and line emission also greatly affects the EWs. (*b*) Difference in EWs, ΔEW, vs. the objective-prism EW, EW_{KISS}. The dashed line indicates $\Delta EW = 0$. The EW difference increases for objects with greater EW_{KISS}; however, the fractional difference $\Delta EW/EW_{KISS}$ remains roughly constant throughout the range of EW_{KISS}.

the ratio of the two fluxes versus the objective-prism fluxes (Fig. 8*b*) shows no apparent systematics.

Figure 9 compares the [N II]-corrected objective-prism EWs to the corresponding long-slit EWs. Again, we see that these quantities agree well; there is no systematic offset between the two distinct measurements. However, we note the relatively large scatter evident in Figures 8 and 9. For example, in the EW comparison plot we see that the scatter is of the same order as the measured EWs. To some degree this scatter is to be expected; the spatial extent of the regions from which the spectra are derived is not the same for the two sets of observations. The objective-prism spectra are extracted from a region corresponding to 8″ in width. Furthermore, since they are slitless, emission from any part of the galaxy that lies above or below the center of the extraction region along the dispersion direction can contribute to the measured emission-line flux. By comparison, the MDM slit is only 1.″68 wide. When an object that is a point source in both line and continuum emission is observed, the resulting flux and EW should be the same for both the objective-prism spectrum and the long-slit spectrum, but for extended objects different amounts of line and continuum emission are detected. For a spatially resolved object in which the line emission is primarily coming from a small, centrally located region, the objective-prism spectrum includes a larger fraction of continuum emission than the long-slit spectrum, and the objective-prism EW is lower than the long-slit EW.

It is important to note that in spite of the large scatter we see when we compare line fluxes and EWs from the survey database to those from the MDM follow-up observations, the *overall* distribution of these properties is very similar. For example, selecting the objects with (uncorrected) objective-prism line fluxes above the median value of 8.6×10^{-15} ergs s^{-1} cm^{-2} produces a sample that includes ~75% of the high-flux objects as selected from the follow-up observations. The same test for the EWs yields similar results; ~75% of the objects found from long-slit spectroscopy to have EWs above the median value would be included if we selected the sample based on the survey EWs.

5. CONCLUSIONS

We have presented the data from follow-up spectroscopy of a sample of 315 emission-line galaxy (ELG) candidates from the KPNO International Spectroscopic Survey (KISS). We verify that all but 7% of this sample consists of extragalactic emission-line objects. The long-slit spectra provide redshift information, line fluxes, equivalent widths (EWs), and optical reddening estimates. Based on the spectral properties, we have classified the objects as starburst galaxies or various types of active galaxies. AGNs account for 13% of the confirmed ELGs. We have also compared the redshifts, Hα line fluxes, and EWs measured in the MDM follow-up spectra to corresponding data derived from the KISS objective-prism spectra. The objective-prism redshifts of the extragalactic emission-line sources agree well with the

redshifts determined from long-slit spectra, except for a few objects in which a shorter wavelength line had been redshifted into the survey bandpass. The Hα fluxes and EWs also show an overall agreement between survey and follow-up data; the scatter that is present is partly due to the fact that the follow-up observations sample different spatial regions of the galaxies.

When added to the previous spectroscopic results from Wegner et al. (2003), the observations in the current paper bring the total number of KISS ELGs observed at MDM to 666, which is nearly 41% of all our existing follow-up spectra. It is our goal to publish all these follow-up spectra as soon as possible to help facilitate the wide scope of scientific inquiry that is possible with a deep survey like KISS. Examples of existing applications of the KISS catalog include the measurement of accurate nebular abundances for low-metallicity ELGs (Melbourne et al. 2004; Lee et al. 2004), the determination of the luminosity-metallicity relation for star-forming galaxies in the local universe (Melbourne & Salzer 2002; Salzer et al. 2005b), the search for local analogs to the luminous compact blue galaxies seen in great numbers at high redshift (Werk et al. 2004), the study of the interstellar medium in dwarf star-forming galaxies (Lee et al. 2002), the radio continuum emission characteristics of star-forming galaxies and AGNs (Van Duyne et al. 2004), and the soft X-ray properties of a complete sample of Seyfert galaxies (Stevenson et al. 2002). The combination of the KISS catalog of ELGs and our growing database of follow-up spectra is a powerful one indeed. It is made all the more powerful when combined with existing wide-field multiwavelength surveys such as FIRST, the NRAO VLA Sky Survey, *IRAS*, the Two Micron All Sky Survey, and *ROSAT*. We expect that the list of projects carried out using the KISS data set will increase tremendously in the coming years.

We gratefully acknowledge financial support for the KISS project from an NSF Presidential Faculty Award to J. J. S. (NSF AST 95-53020), as well as continued support for our ongoing follow-up spectroscopy campaign (NSF AST 00-71114 and NSF AST 03-07766). We also thank Wesleyan University for providing additional funding for the observing runs during which these follow-up spectral data were obtained. Finally, we wish to thank Bob Barr of MDM Observatory for his excellent assistance in maintaining the telescope and instrumentation used for these observations.

REFERENCES

Baldwin, J. A., Phillips, M. M., & Terlevich, R. 1981, PASP, 93, 5
Dopita, M. A., & Evans, I. N. 1986, ApJ, 307, 431
Gronwall, C., Jangren, A., Salzer, J. J., Werk, J., & Ciardullo, R. 2004a, AJ, 128, 644
Gronwall, C., Salzer, J. J., Sarajedini, V. L., Jangren, A., Chomiuk, L. B., Moody, J. W., Frattare, L. M., & Boroson, T. A. 2004b, AJ, 127, 1943 (KR2)
Gronwall, C., Sarajedini, V. L., & Salzer, J. J. 2002, in IAU Colloq. 184, AGN Surveys, ed. R. F. Green, E. Ye. Khachikian, & D. B. Sanders (ASP Conf. Ser. 284; San Francisco: ASP), 43
Kennicutt, R. C., Jr. 1992, ApJ, 388, 310
Kennicutt, R. C., Jr., & Kent, S. M. 1983, AJ, 88, 1094
Lee, J. C., Salzer, J. J., Impey, C., Thuan, T. X., & Gronwall, C. 2002, AJ, 124, 3088
Lee, J. C., Salzer, J. J., & Melbourne, J. 2004, ApJ, 616, 752
Melbourne, J., Phillips, A. C., Salzer, J. J., Gronwall, C., & Sarajedini, V. L. 2004, AJ, 127, 686
Melbourne, J., & Salzer, J. J. 2002, AJ, 123, 2302
Osterbrock, D. E. 1989, Astrophysics of Gaseous Nebulae and Active Galactic Nuclei (Mill Valley: University Science Books)
Salzer, J. J., Jangren, A., Gronwall, C., Chomiuk, L. B., Caperton, K. A., Melbourne, J., & McKinstry, K. 2005a, AJ, submitted
Salzer, J. J., Lee, J. C., Melbourne, J., Hinz, J., Alonso-Herrero, A., & Jangren, A. 2005b, ApJ, 624, 661
Salzer, J. J., et al. 2000, AJ, 120, 80 (Paper I)
———. 2001, AJ, 121, 66 (KR1)
———. 2002, AJ, 123, 1292 (KB1)
Stevenson, S., Salzer, J. J., Sarajedini, V. L., & Moran, E. C. 2002, AJ, 124, 3465
Thorstensen, J. R., Wegner, G. A., Hamwey, R., Boley, F., Geller, M. J., Juchra, J. P., Kurtz, M. J., & McMahan, R. K. 1989, AJ, 98, 1143
Van Duyne, J., Beckerman, E., Salzer, J. J., Gronwall, C., Thuan, T. X., Condon, J. J., & Frattare, L. M. 2004, AJ, 127, 1959
Veilleux, S., & Osterbrock, D. E. 1987, ApJS, 63, 295
Wegner, G., Salzer, J. J., Jangren, A., Gronwall, C., & Melbourne, J. 2003, AJ, 125, 2373
Wegner, G., et al. 2001, AJ, 122, 2893
Werk, J. K., Jangren, A., & Salzer, J. J. 2004, ApJ, 617, 1004